

## Article

# Sensitivity-Enhanced, Room-Temperature Detection of NH<sub>3</sub> with Alkalized Ti<sub>3</sub>C<sub>2</sub>T<sub>x</sub> MXene

Yi Tan <sup>1</sup>, Jinxia Xu <sup>1,2,\*</sup> , Qiliang Li <sup>3,\*</sup> , Wanting Zhang <sup>1</sup>, Chong Lu <sup>1</sup>, Xingjuan Song <sup>1</sup>, Lingyun Liu <sup>1,2</sup> and Ying Chen <sup>1,2</sup> 

<sup>1</sup> School of Science, Hubei University of Technology, Wuhan 430068, China; 102112284@hbut.edu.cn (Y.T.); 102202245@hbut.edu.cn (W.Z.); 102312420@hbut.edu.cn (C.L.); xingjuansong@hbut.edu.cn (X.S.); liulingyun@mail.hbut.edu.cn (L.L.); chenyddc@163.com (Y.C.)

<sup>2</sup> Hubei Key Laboratory for High-Efficiency Utilization of Solar Energy and Operation Control of Energy Storage System, Hubei University of Technology, Wuhan 430068, China

<sup>3</sup> Department of Advanced Manufacturing and Robotics, College of Engineering, Peking University, Beijing 100871, China

\* Correspondence: xujx@hbut.edu.cn (J.X.); qiliang.li@pku.edu.cn (Q.L.)

**Abstract:** A layered Ti<sub>3</sub>C<sub>2</sub>T<sub>x</sub> MXene structure was prepared by etching MAX-phase Ti<sub>3</sub>AlC<sub>2</sub> with hydro-fluoric acid (HF), followed by alkalization in sodium hydroxide (NaOH) solutions of varying concentrations and for varying durations. Compared to sensors utilizing unalkalized Ti<sub>3</sub>C<sub>2</sub>T<sub>x</sub>, those employing alkalized Ti<sub>3</sub>C<sub>2</sub>T<sub>x</sub> MXene exhibited enhanced sensitivity for NH<sub>3</sub> detection at room temperature and a relative humidity of 40%. Both the concentration of NaOH and duration of alkalization significantly influenced sensor performance. Among the tested conditions, Ti<sub>3</sub>C<sub>2</sub>T<sub>x</sub> MXene alkalized with a 5 M NaOH solution for 12 h exhibited optimal performance, with high response values of 100.3% and a rapid response/recovery time of 73 s and 38 s, respectively. The improved sensitivity of NH<sub>3</sub> detection can be attributed to the heightened NH<sub>3</sub> adsorption capability of oxygen-rich terminals obtained through the alkalization treatment. This is consistent with the observed increase in the ratio of oxygen to fluorine atoms on the surface terminations of the alkalization-treated Ti<sub>3</sub>C<sub>2</sub>T<sub>x</sub>. These findings suggest that the gas-sensing characteristics of Ti<sub>3</sub>C<sub>2</sub>T<sub>x</sub> MXene can be finely tuned and optimized through a carefully tailored alkalization process, offering a viable approach to realizing high-performance Ti<sub>3</sub>C<sub>2</sub>T<sub>x</sub> MXene gas sensors, particularly for NH<sub>3</sub> sensing applications.

**Keywords:** Ti<sub>3</sub>C<sub>2</sub>T<sub>x</sub> MXene; alkalization; NH<sub>3</sub> sensing; room temperature



**Citation:** Tan, Y.; Xu, J.; Li, Q.; Zhang, W.; Lu, C.; Song, X.; Liu, L.; Chen, Y. Sensitivity-Enhanced, Room-Temperature Detection of NH<sub>3</sub> with Alkalized Ti<sub>3</sub>C<sub>2</sub>T<sub>x</sub> MXene. *Nanomaterials* **2024**, *14*, 680. <https://doi.org/10.3390/nano14080680>

Academic Editor: Francesc Viñes Solana

Received: 18 March 2024

Revised: 11 April 2024

Accepted: 11 April 2024

Published: 15 April 2024



**Copyright:** © 2024 by the authors. Licensee MDPI, Basel, Switzerland. This article is an open access article distributed under the terms and conditions of the Creative Commons Attribution (CC BY) license (<https://creativecommons.org/licenses/by/4.0/>).

## 1. Introduction

Gas sensors have found widespread applications in various fields such as food safety, medical diagnosis, and hazardous gas monitoring due to their ability to track invisible environmental information [1–3]. To date, a variety of materials, such as nanoparticles, metal oxide semiconductors, and 2D materials, have been used to fabricate gas sensors [4,5]. Among these materials, metal oxides are extensively utilized in gas detection owing to their high sensitivity, excellent stability, and low cost [6–8]. Nevertheless, achieving optimal performance with metal oxide semiconductor sensors typically requires high operating temperatures, leading to substantial energy consumption. This poses a critical limitation for integrated circuits and the Internet of Things [9]. Hence, it is necessary to develop new gas-sensitive materials capable of operating at room temperature (RT).

Ammonia (NH<sub>3</sub>), widely used in industry, agriculture, and various other sectors, is a harmful air pollutant. NH<sub>3</sub> not only threatens the stability of water ecosystems but also contributes to the formation of suspended particles in the atmosphere [10,11]. Even at low concentrations, NH<sub>3</sub> can have adverse effects on human health, leading to symptoms such as vomiting, headaches, and pulmonary edema. Therefore, it is imperative to monitor the concentration of ammonia in the air. Moreover, detecting the concentration of NH<sub>3</sub> in

exhaled breath, generated through metabolic activities in the human body, can effectively diagnose diseases such as kidney disorders. Therefore, the development of an  $\text{NH}_3$  gas sensor capable of operating at room temperature under atmospheric humidity conditions with high sensitivity and a low detection limit is crucial.

MXenes, compounds consisting of transition metal carbides, nitrides, and carbonitrides, similar to graphene-like layered materials, have shown attractive applications across various fields. These applications include gas sensing, energy storage, and water purification, owing to MXenes' excellent electronic, optical, mechanical, and thermal properties [12,13]. In particular, MXenes were reported to be promising sensing materials in gas sensors, primarily due to their high specific surface area, elevated electrical conductivity, abundant surface functional terminal groups, and efficient operation at RT [14,15]. The development of MXene-based gas sensors with high selectivity and sensitivity has attracted more and more attention as a prominent focus within gas sensor research [16–18]. In general, MXenes are prepared by etching the aluminum layer in MAX with HF or a mixed solution of HCl and LiF. Although the use of the mixed HCl and LiF solutions is safer in comparison to HF, MXenes prepared with this mixed solution show compact structures without significant delamination [19,20]. However, MXenes prepared with HF etching show a remarkable layered structure, making them more conducive to gas sensitivity. Additionally, the layered structure obtained with HF etching is highly stable [21–23]. According to previous reports, the -O and -OH surface functional terminal groups play key roles in gas detection [14,24]. However, MXenes prepared with HF etching possess a higher concentration of -F functional groups on their surface. Enhanced electrochemical performance has been achieved by reducing these -F terminal groups using various post-processing methods [25–27]. In this work, a simple and yet effective approach was employed to modify the functional terminal groups and expand the interlayers of  $\text{Ti}_3\text{C}_2\text{T}_x$  MXene through alkalization. Zhang et al. reported that the alkalization-grafting modification of amino-functionalized  $\text{Ti}_3\text{C}_2\text{T}_x$  MXene nanosheets yielded a highly efficient adsorption capacity for lead ions [28]. Liang et al. reported that mesoporous  $\gamma\text{-Fe}_2\text{O}_3$  nanospheres @ $\text{Ti}_3\text{C}_2\text{T}_x$  MXene treated with LiOH showed enhanced lithium storage capabilities [29]. Bae et al. reported that the electrical properties of  $\text{Ti}_3\text{C}_2\text{T}_x$  MXene could be modified by NaOH alkalization, leading to a transition from -F terminations to -OH/-O terminations [30]. Yang et al. reported that layered  $\text{Ti}_3\text{C}_2\text{T}_x$  MXene treated with NaOH showed enhanced gas and humidity sensitivity performance owing to the increasing ratio of oxygen to fluorine functional terminal groups [31]. However, the effect of NaOH concentrations and alkalization time on the performance of  $\text{NH}_3$  detection has not been studied. In this work, gas sensors were fabricated based on  $\text{Ti}_3\text{C}_2\text{T}_x$  MXene alkalized with various concentrations of NaOH for different durations, and their  $\text{NH}_3$  gas-sensing performance at RT was investigated. Moreover, the mechanism of the sensing performance of the prepared sensors was also discussed. Our results indicate that the alkalization treatment of  $\text{Ti}_3\text{C}_2\text{T}_x$  MXene is a simple and effective method for enhancing  $\text{NH}_3$  gas sensing at RT. This improvement is crucial for the practical application of  $\text{Ti}_3\text{C}_2\text{T}_x$  MXene in gas sensor technology.

## 2. Materials and Methods

### 2.1. Preparation of $\text{Ti}_3\text{C}_2\text{T}_x$ MXene

Figure 1a illustrates the schematic preparation process of  $\text{Ti}_3\text{C}_2\text{T}_x$  MXene and the alkalization of  $\text{Ti}_3\text{C}_2\text{T}_x$  MXene by NaOH. First, 1 g of  $\text{Ti}_3\text{AlC}_2$  was added into a solution of 20 mL 40 wt% HF, and then continuously stirred for 24 h at 40 °C in a water bath using a magnetic stirrer. After etching, the precipitates were filtered and cleaned with deionized water by centrifugation several times (about 5 to 6 times) until reaching  $\text{pH} \approx 7$ . Next, the residue was dried at 50 °C for 24 h in a vacuum oven. Finally, the layered-structure  $\text{Ti}_3\text{C}_2\text{T}_x$  MXene was successfully prepared.

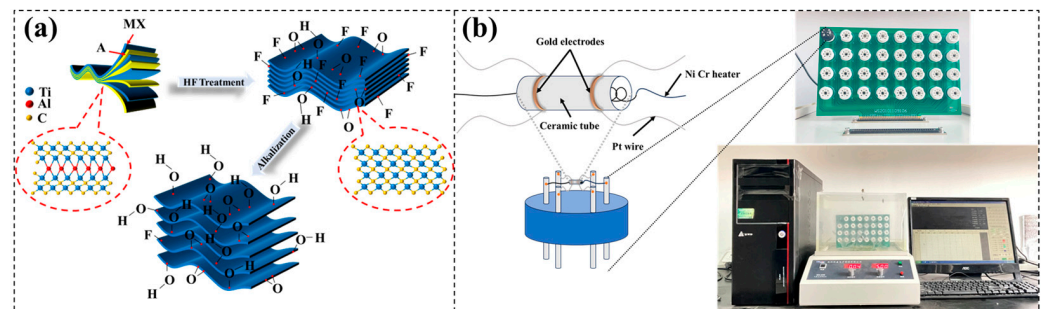


**Figure 1.** (a) Schematic diagram of the preparation process of alkalinized  $Ti_3C_2T_x$  MXene. (b) Schematic diagram of the preparation and measurement of gas sensors.

### 2.2. Preparation of Alkalinized $Ti_3C_2T_x$ MXene

Furthermore, 0.5 g of prepared  $Ti_3C_2T_x$  MXene was added into a 30 mL 2/5/8 M NaOH solution, and then the mixture was stirred for 6, 12, 18, 24 h, respectively, at RT and RH of 40%. Subsequently, the precipitates were filtered and cleaned with deionized water by centrifugation several times until a pH  $\approx$  7 was achieved. The residue was then dried at 50 °C for 24 h in a vacuum oven. As a result,  $Ti_3C_2T_x$  MXene with different degrees of alkalization were successfully prepared.

### 2.3. Characterization

The morphologies of pristine and alkalinized  $Ti_3C_2T_x$  MXene were characterized using field-emission scanning electron microscopy (FESEM, JEOL JSM-7500F, Tokyo, Japan) with an acceleration voltage of 15 kV. Additionally, the elemental contents of all samples were analyzed by energy-dispersive X-ray spectroscopy (EDS) attached to the SEM device. Structural characterization was performed using X-ray diffraction (XRD, Rigaku D/Max 2550, Tokyo, Japan) with Cu K $\alpha$  radiation ( $\lambda = 1.5418 \text{ \AA}$ ) over a scanning range of 5–80°. Elemental chemical status and compositions were determined using X-ray photoelectron spectroscopy (XPS) with Al K $\alpha$  (1486.6 eV) excitation.

### 2.4. Fabrication and Measurement of Gas Sensors

The schematic diagram of the preparation and measurement of the gas sensor is shown in Figure 1b. The prepared MXene or alkalization-treated MXene were mixed with ethanol to form a slurry, which was then applied onto an alumina ceramic tube. Subsequently, the alumina ceramic tube was dried in a vacuum oven at 50 °C for 24 h. To further enhance its structural stability, the alumina ceramic was aged in air at RT for an additional 24 h. Gas-sensing performance was evaluated using a WS-30B measuring system (Winsen Electronics Technology Co., Ltd., Zhengzhou, China) with an 18 L sensing chamber at RT and relative humidity (RH) of 40%, employing a static gas testing method. The testing gas was generated by heating a liquid into vapor. The valve formula for measuring the volume of liquid vapor was as follows:

$$V_x = \frac{V \times C \times M}{22.4 \times d \times p} \times 10^{-9} \times \frac{273 + T_r}{273 + T_b}$$

where  $V$  (mL) is the volume of the test box;  $C$  (ppm) is the liquid vapor concentration, in parts per million;  $M$  is the liquid molecular weight;  $d$  ( $g/cm^3$ ) is the specific gravity of the liquid, in grams per cubic centimeter;  $p$  is the liquid purity;  $T_r$  (°C) is room temperature; and  $T_b$  (°C) is the temperature in the test box.

The sensor response (Sg) can be calculated using the formula  $Sg = [(R_g - R_a)/R_a] \times 100\%$ , where  $R_a$  represents the resistance of the sensor in air and  $R_g$  represents the resistance of the sensor in the target gas. The response and recovery characteristics, repeatability, and stability of the sensors were evaluated under identical conditions.

### 3. Results and Discussion

Figure 1a shows a schematic diagram of the process of preparing alkalinized  $\text{Ti}_3\text{C}_2\text{T}_x$  MXene. After the removal of the Al layer by HF etching, the surface of the  $\text{Ti}_3\text{C}_2\text{T}_x$  MXene is mainly composed of -F, -O, and -OH functional terminations. After alkalization, mainly -O and -OH surface groups remain with -F-rich surface terminations being transformed to -O- and -OH-rich terminations. The XRD patterns of  $\text{Ti}_3\text{AlC}_2$ ,  $\text{Ti}_3\text{C}_2\text{T}_x$ , and alkalization-treated  $\text{Ti}_3\text{C}_2\text{T}_x$  MXene using 2/5/8 M NaOH for 12 h are presented in Figure 2a,b. Figure 2c–e show the SEM images of  $\text{Ti}_3\text{AlC}_2$ ,  $\text{Ti}_3\text{C}_2\text{T}_x$ , and alkalization-treated  $\text{Ti}_3\text{C}_2\text{T}_x$  MXene using 5 M NaOH for 12 h, respectively. As shown in Figure 2a, for the  $\text{Ti}_3\text{AlC}_2$ , distinct peaks were observed at  $2\theta$  values of  $9.52^\circ$ ,  $19.13^\circ$ ,  $34.03^\circ$ ,  $36.06^\circ$ ,  $39.8^\circ$ , and  $41.84^\circ$ ; these peaks corresponded to the (002), (004), (101), (103), (104), (105), and (110) lattice planes, respectively. But after HF etching, only (002) diffraction peak appears in the  $\text{Ti}_3\text{C}_2\text{T}_x$  MXene' XRD pattern, the (104) diffraction peak disappears due to the removal of the Al layer, and the other peaks disappear as well [32,33]. Also, the (002) peak is shifted to a lower angle in comparison to that of the  $\text{Ti}_3\text{AlC}_2$ , suggesting an increase in interlayer spacing due to the extraction of the Al layer [9]. As shown in Figure 2b and the inset, after alkalization treatment, the typical diffraction peak of (002) is clearly shifted to a lower angle, from  $6.35^\circ$  to  $5.74^\circ$ , with the increase in the NaOH solution's concentration. This indicates that the  $\text{Na}^+$  metal ion double stack incorporated into the MXene layer causes an increase in the lattice constant as well as the interlayer spacing [34]. With the increase in the NaOH solution's concentration, both the number of incorporated  $\text{Na}^+$  metal ions and the replacement of surface terminations with -OH functional groups increase, which is clearly observed in the increasing interlayer spacing. This result is in agreement with the previous literature [30,34–36]. The increase in the interlayer spacing may be one of the major reasons causing the MXenes' enhanced gas-sensing performance. In addition, the SEM results indicate that the dense layered structure of  $\text{Ti}_3\text{AlC}_2$  was transformed into a layered structure due to the removal of the Al layer after being etched in the HF solution, which proves that the  $\text{Ti}_3\text{C}_2\text{T}_x$  layered structure was successfully prepared. After being alkalized in 5 M NaOH for 12 h, the alkalized  $\text{Ti}_3\text{C}_2\text{T}_x$  MXene structure shows larger stacking gaps. The SEM results are consistent with the XRD results. This layered morphology of the MXenes may play a significant role in their gas-sensing performance.

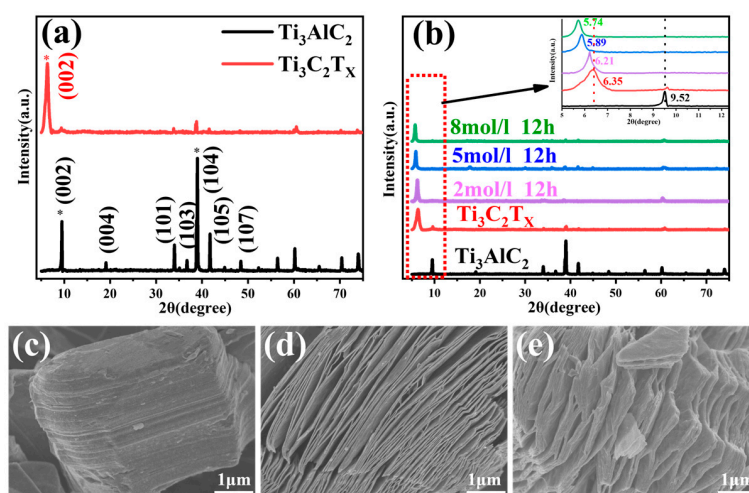


**Figure 2.** XRD patterns of (a)  $\text{Ti}_3\text{AlC}_2$  and  $\text{Ti}_3\text{C}_2\text{T}_x$ ; (b)  $\text{Ti}_3\text{C}_2\text{T}_x$  MXene alkalized with 2/5/8 M NaOH for 12 h. SEM images of (c)  $\text{Ti}_3\text{AlC}_2$ ; (d)  $\text{Ti}_3\text{C}_2\text{T}_x$ ; and (e)  $\text{Ti}_3\text{C}_2\text{T}_x$  MXene alkalized with 5 M NaOH for 12 h.

Figure 3 shows the dynamic sensing characteristics of the  $\text{Ti}_3\text{C}_2\text{T}_x$  MXene produced with different alkalization processes upon exposure to  $\text{NH}_3$  in a ppm concentration range of 5–500 ppm at RT and an RH of 40%. As shown in Figure 3a–c, the sensitivities of the

alkalized  $\text{Ti}_3\text{C}_2\text{T}_x$  MXene sensors are clearly enhanced in comparison with those built of pristine MXene. The response magnitude of alkalinized  $\text{Ti}_3\text{C}_2\text{T}_x$  MXene sensors increases with the increase in the  $\text{NH}_3$  concentration from 5 ppm to 500 ppm, while the sensors based on MXene undergoing 12 h of alkalization exhibit the highest response. Figure 3d shows the dynamic sensing characteristics of alkalization with 2/5/8 M NaOH for 12 h, among which the  $\text{Ti}_3\text{C}_2\text{T}_x$  MXene sensor alkalinized by 5 M NaOH has the highest response; the response value of this sensor is improved by 4 to 11 times compared to the  $\text{Ti}_3\text{C}_2\text{T}_x$ -based sensors, and the device achieves detection at 5 ppm. This analysis demonstrates the best combination of NaOH concentration and alkalization time for optimal sensing performance. Thus, the  $\text{Ti}_3\text{C}_2\text{T}_x$  MXene sensor alkalinized with 5 M NaOH for 12 h has excellent performance and was selected for the subsequent investigation.

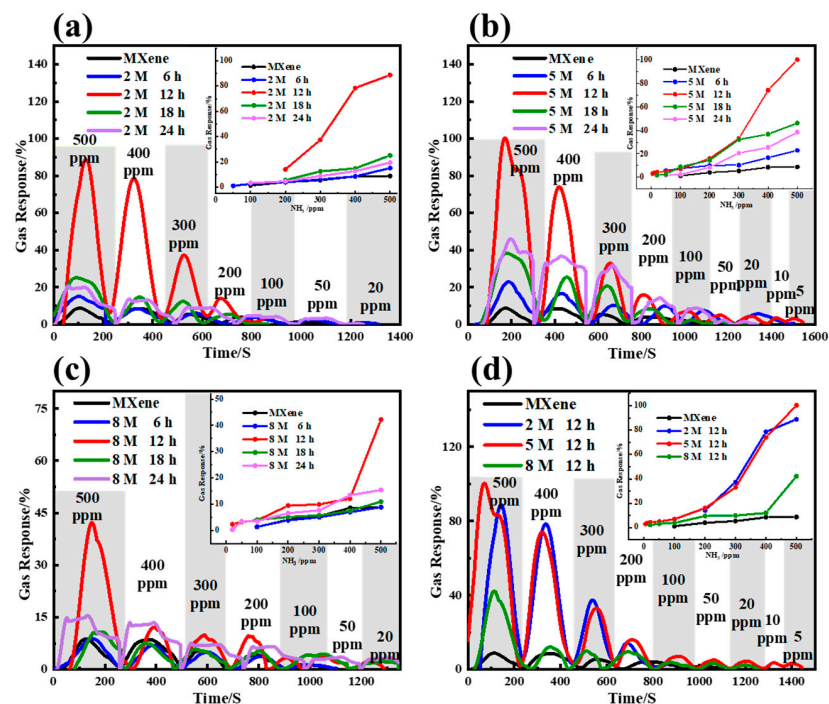


**Figure 3.** Dynamic sensing characteristics of the  $\text{Ti}_3\text{C}_2\text{T}_x$  MXene with different degrees of alkalization upon exposure to  $\text{NH}_3$  in ppm concentration range of 5–500 ppm at RT and RH of 40%: (a) 2 M NaOH for 6 h, 12 h, 18 h, 24 h; (b) 5 M NaOH for 6 h, 12 h, 18 h, 24 h; (c) 8 M NaOH for 6 h, 12 h, 18 h, 24 h; (d) 2/5/8 M NaOH for 12 h.

The response–recovery behavior is crucial for gas sensor performance. The response and recovery times can be defined and calculated based on the characteristics of response–recovery transients. Figure 4 displays the response–recovery curves of the sensors fabricated with pristine MXene and alkalinized  $\text{Ti}_3\text{C}_2\text{T}_x$  MXene treated with 5 M NaOH for 12 h upon exposure to 200 ppm of  $\text{NH}_3$  at RT and an RH of 40%. The response time is described as the required time for the vibrational resistance to reach 90% of the stable resistance subsequent to the injecting of target gas. The recovery time is defined as the necessary time for the sensor to recover 90% of the changed resistance value in the air after releasing the target gas. As shown in Figure 4a, the gas-in switch is turned on at  $t = 13$  s, causing an abrupt increase in sensor resistance in response to the injection of the ammonia gas. The sensor resistance is stabilized at  $t = 112$  s, experiencing an increase from  $396 \Omega$  to  $427 \Omega$ . The response time can be characterized as the period from gas-in to the time when the resistance reaches 90% of the saturation value ( $425 \Omega$ ) at  $t = 96$  s. Therefore, the response time was calculated as  $96 \text{ s} - 13 \text{ s} = 83 \text{ s}$ . At  $t = 240$  s, air is introduced into the measurement, causing a decrease in resistance from  $422 \Omega$  to  $402 \Omega$ . The recovery time is described as the period from air-in to the time when the resistance decreases to 90% saturation resistance ( $404 \Omega$ ) at  $t = 324$  s. Therefore, the recovery time was  $324 \text{ s} - 240 \text{ s} = 84 \text{ s}$ . So, the response time to ammonia

gas is 83 s, and the recovery time is 84 s for the pristine  $\text{Ti}_3\text{C}_2\text{T}_x$  MXene sensor at RT and an RH of 40%. Through a similar experiment on the sensor based on  $\text{Ti}_3\text{C}_2\text{T}_x$  MXene alkalinized with 5 M NaOH for 12 h, the response and recovery times were calculated as 73 s and 38 s, respectively, upon exposure to ammonia gas at RT and an RH of 40%. The results indicate that the sensors based on alkalinized  $\text{Ti}_3\text{C}_2\text{T}_x$  MXene have much shorter response and recovery times compared to the sensors fabricated with pristine  $\text{Ti}_3\text{C}_2\text{T}_x$  MXene. The observed improvement in the ammonia gas response of alkalinized  $\text{Ti}_3\text{C}_2\text{T}_x$  MXene sensors can be attributed to the enhanced capability to absorb and desorb ammonia gas on the surface of the alkalinized  $\text{Ti}_3\text{C}_2\text{T}_x$  MXene. The details of this will be discussed later. Moreover, repeatability and stability are also important features for practical applications. Figure 4c,d show the repeatability of the sensors based on  $\text{Ti}_3\text{C}_2\text{T}_x$  MXene and  $\text{Ti}_3\text{C}_2\text{T}_x$  MXene alkalinized with 5 M NaOH for 12 h in response to 200 ppm of  $\text{NH}_3$  for five cycles at RT and an RH of 40%, respectively. The resistance of  $\text{Ti}_3\text{C}_2\text{T}_x$  MXene and alkalinized  $\text{Ti}_3\text{C}_2\text{T}_x$  MXene displayed an increase and decrease along with the change in ammonia concentration. The resistance of pristine  $\text{Ti}_3\text{C}_2\text{T}_x$  MXene did not return to the base resistance, showing base resistance drift, while the change in the resistance of the alkalinized  $\text{Ti}_3\text{C}_2\text{T}_x$  MXene sensor was able to return to the base resistance; only a very small variation can be observed in sensor response, indicating a good reproducibility. As shown in Figure 4e,f, long-term stability was also observed in the sensors based on pristine  $\text{Ti}_3\text{C}_2\text{T}_x$  and  $\text{Ti}_3\text{C}_2\text{T}_x$  MXene alkalinized with 5 M NaOH for 12 h upon exposure to 200 ppm of  $\text{NH}_3$  for about 17 days at RT and an RH of 40%, respectively. The fluctuation in the response values of the alkalinized  $\text{Ti}_3\text{C}_2\text{T}_x$  MXene (30%) is smaller than that of the pristine MXene sensor (60%), which proves that alkalinized MXene has good long-term stability.

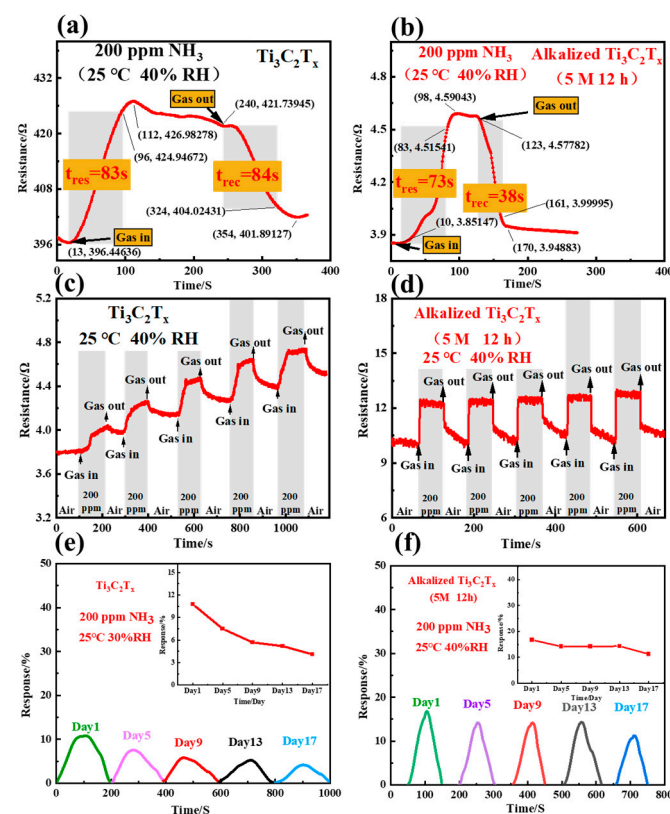


**Figure 4.** Response–recovery curves of (a) pristine  $\text{Ti}_3\text{C}_2\text{T}_x$  MXene sensor and (b)  $\text{Ti}_3\text{C}_2\text{T}_x$  MXene sensor alkalinized with 5 M NaOH for 12 h exposed to 200 ppm of  $\text{NH}_3$  at RT and RH of 40%; (c) the repeatability of  $\text{Ti}_3\text{C}_2\text{T}_x$  MXene sensor to 200 ppm of  $\text{NH}_3$  for 5 cycles at RT and RH of 40%; (d) the repeatability of  $\text{Ti}_3\text{C}_2\text{T}_x$  MXene sensor alkalinized with 5 M NaOH for 12 h to 200 ppm of  $\text{NH}_3$  for 5 cycles at RT and RH of 40%; (e) long-term stability of  $\text{Ti}_3\text{C}_2\text{T}_x$  MXene sensor to 200 ppm of  $\text{NH}_3$  for about 17 days at RT and RH of 40%; (f) long-term stability of  $\text{Ti}_3\text{C}_2\text{T}_x$  MXene sensor alkalinized with 5 M NaOH for 12 h to 200 ppm of  $\text{NH}_3$  for about 17 days at RT and RH of 40%.

In order to evaluate the performance of the alkalized  $\text{Ti}_3\text{C}_2\text{T}_x$  MXene sensor, the RT gas-sensing parameters of the present study were compared with those of other  $\text{NH}_3$  sensors from previous reports, as shown in Table 1. It can be observed that the gas-sensing performance in the present study is better than other listed reports in terms of the response value. Hence,  $\text{Ti}_3\text{C}_2\text{T}_x$  MXene treated with the alkalization method is a simple and effective approach to enhance the performance of  $\text{NH}_3$  detection at RT.

**Table 1.** Comparison of RT  $\text{NH}_3$ -sensing properties in the present work and other literature.

Materials	$\text{NH}_3$ (ppm)	Response (%)	Response/Recovery Time	Ref.
$\text{Ti}_3\text{C}_2\text{T}_x$	100	0.21	-	[9]
$\text{Ti}_3\text{C}_2\text{T}_x$	100	0.8	-	[37]
$\text{Ti}_3\text{C}_2\text{T}_x$	100	0.12	6.8/13.3 min (100 ppm $\text{NH}_3$ )	[38]
$\text{Ti}_3\text{C}_2\text{T}_x/\text{Graphene}$	100	6.77	3/12 min (100 ppm $\text{NH}_3$ )	[39]
3D $\text{Ti}_3\text{C}_2\text{T}_x$	100	0.8	1.5/1.7 min (5 ppm $\text{NH}_3$ )	[40]
$\text{Ti}_3\text{C}_2\text{T}_x/\text{SnO}_2$	100	3.1	109/342 s (100 ppm $\text{NH}_3$ )	[41]
MXene/ $\text{TiO}_2$ /cellulose	100	6.84	76/62 s (100 ppm $\text{NH}_3$ )	[42]
Alkalized $\text{Ti}_3\text{C}_2\text{T}_x$	100	7.04	73/38 s (200 ppm $\text{NH}_3$ )	This work
Single-layer $\text{Ti}_3\text{C}_2\text{T}_x$	500	6.13	45/94 s (25 ppm $\text{NH}_3$ )	[43]
$\text{Ti}_3\text{C}_2\text{T}_x$ MXene/ $\text{MoS}_2$	500	5.8	-	[44]
Alkalized $\text{Ti}_3\text{C}_2\text{T}_x$	500	78	-	[31]
Alkalized $\text{Ti}_3\text{C}_2\text{T}_x$	500	100.3	73/38 s (200 ppm $\text{NH}_3$ )	This work

The charge transfer mechanism of the  $\text{NH}_3$  molecules' adsorption/desorption process and electrical conductivity changes is shown in Figure 5. In general,  $\text{Ti}_3\text{C}_2\text{T}_x$  MXene is a p-type semiconductor wherein holes serve as the main conductive carriers, and alkalized  $\text{Ti}_3\text{C}_2\text{T}_x$  MXene also exhibits a p-type sensing behavior [16]. Therefore, the gas-sensing mechanism relies on the charge transfer during the adsorption and desorption of  $\text{NH}_3$  on the surface of the  $\text{Ti}_3\text{C}_2\text{T}_x$  MXene. When the  $\text{Ti}_3\text{C}_2\text{T}_x$  MXene sensor is exposed to an  $\text{NH}_3$  atmosphere, the  $\text{NH}_3$  will react with the -O and -OH surface terminals to form  $\text{NH}_2$ ,  $\text{N}_2$ , and  $\text{H}_2\text{O}$  and release electrons to the conduction band of the  $\text{Ti}_3\text{C}_2\text{T}_x$  MXene. The hole conductive channel can be thinned to correspondingly increase the resistance [45]. Meanwhile, when exposed to air, oxygen molecules will capture electrons from the surface of the  $\text{Ti}_3\text{C}_2\text{T}_x$  MXene, generating negative oxygen species like  $\text{O}_2^-$  (at RT), resulting in the thickening of the hole conductive channel and a decrease in resistance [43,46,47]. The charge transfer process shows that -OH and -O are crucial to the adsorption of  $\text{NH}_3$  on the surface of  $\text{Ti}_3\text{C}_2\text{T}_x$  MXene sensors.

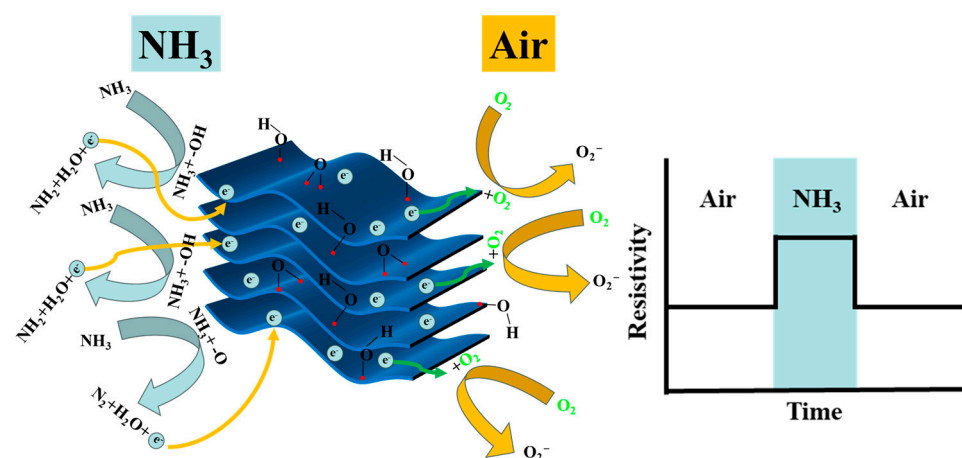


**Figure 5.** Schematic diagram of the charge transfer mechanism and electrical conductivity changes in  $\text{NH}_3$  and air.

Therefore, the reasons for the enhanced  $\text{NH}_3$  sensitivity of gas sensors based on alkali-ized  $\text{Ti}_3\text{C}_2\text{T}_x$  MXene at RT can be explained as follows. Firstly, double-stacked  $\text{Na}^+$  metal ions are incorporated into the MXene layer after alkalization treatment, leading to an increase in the lattice constant and interlayer spacing. This effectively increases the specific surface area and the contact area with  $\text{NH}_3$ , thereby significantly improving the ability of ammonia adsorption. As a result, the  $\text{NH}_3$  sensitivity of the alkali-ized  $\text{Ti}_3\text{C}_2\text{T}_x$  MXene sensor can be greatly enhanced. Zheng et al. reported that a  $\text{Ti}_3\text{C}_2\text{T}_x$  MXene treated by alkaline solution of LiOH, NaOH, and KOH showed an enhanced adsorption performance due to the expanded layer spacing and surface functional groups [48]. Wang et al. designed alkali-ized MXene/ $\text{CoFe}_2\text{O}_4$ /CS layered structures which showed ultra-strong abilities to adsorb CR, RhB, and MG dyes owing to the increased layer spacing of alkali-ized MXene [49]. Lian et al. also reported that alkali-ized  $\text{Ti}_3\text{C}_2$  MXene nanoribbons were attractive for use in high-capacity ion batteries with expanding interlayer spacing [50]. Moreover, structural stability is also important for high sensing performance. The incorporated  $\text{Na}^+$  can effectively prevent the stacking of the  $\text{Ti}_3\text{C}_2\text{T}_x$  MXene [35]. As a result, the MXene can maintain a layered structure with high gas-sensing performance. The stability in sensor response is owed to the stable microstructure of the alkali-ized  $\text{Ti}_3\text{C}_2\text{T}_x$  MXene. Secondly, the  $-\text{F}$  surface functional terminations of  $\text{Ti}_3\text{C}_2\text{T}_x$  MXene are replaced by  $-\text{OH}$  and  $-\text{O}$  functional groups after NaOH alkalization, leading to a higher ratio of oxygen to fluorine atoms of the surface terminals [30,34,51]. The transformation of  $-\text{F}$  to  $-\text{OH}$  and  $-\text{O}$  are demonstrated by the XPS spectra and EDS mapping presented in Figures 6 and 7. This transformation increases the number of available active sites for adsorption, thereby facilitating interactions between the MXene and ammonia, and resulting in the enhancement of the gas-sensing performance [52]. Thirdly,  $-\text{OH}$  functional groups have a negative charge, which is better able to attract positive nitrogen ions in  $\text{NH}_3$  molecules by electrostatic force [45], which will be discussed in detail in the next section.

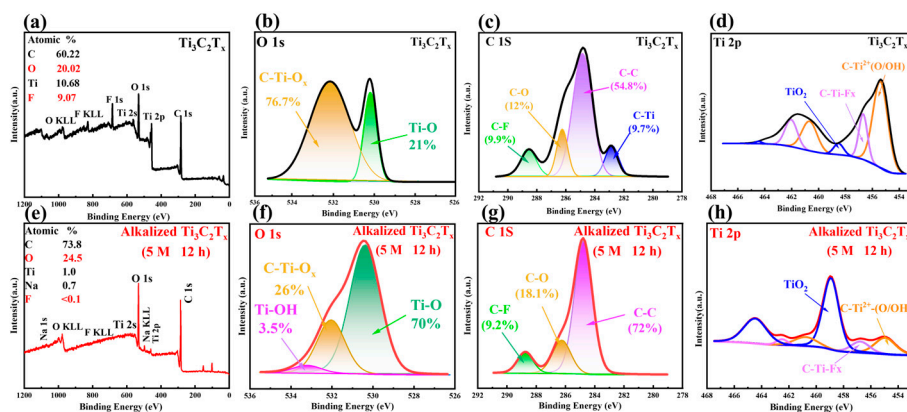


**Figure 6.** XPS spectra of  $\text{Ti}_3\text{C}_2\text{T}_x$  (a–d) and  $\text{Ti}_3\text{C}_2\text{T}_x$  alkali-ized with 5 M NaOH for 12 h (e–h): (a,e) Survey XPS spectra; (b,f) O 1s spectra; (c,g) C 1s spectra; (d,h) Ti 2p spectra of  $\text{Ti}_3\text{C}_2\text{T}_x$  and  $\text{Ti}_3\text{C}_2\text{T}_x$  alkali-ized with 5 M NaOH for 12 h.

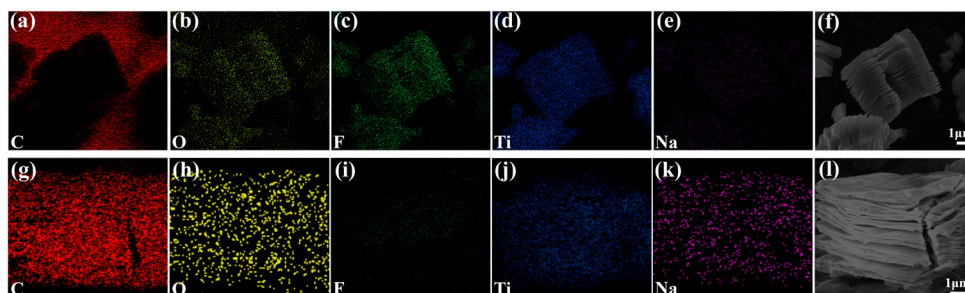


**Figure 7.** The EDS element mapping scanning images of  $\text{Ti}_3\text{C}_2\text{T}_x$  (a–f) and alkali-ized  $\text{Ti}_3\text{C}_2\text{T}_x$  (g–l).

The surface chemical compositions and binding state of the samples of  $\text{Ti}_3\text{C}_2\text{T}_x$  and  $\text{Ti}_3\text{C}_2\text{T}_x$  alkalinized with 5 M NaOH for 12 h were investigated by XPS in detail. The survey XPS spectra of  $\text{Ti}_3\text{C}_2\text{T}_x$  and  $\text{Ti}_3\text{C}_2\text{T}_x$  alkalinized with 5 M NaOH for 12 h show that the intensity of the F 1s peak becomes weaker after alkalization due to transitioning from -F to -OH terminations following alkalization, as shown in Figure 6a,e. The ratio of the number of O to F atoms is about 2.2, with an F content = 9.07 at% and an O content = 20.02 at%. After alkalization, the ratio of O to F atoms is quite high, with the F content decreasing to less than 0.1 at% and O content increasing to 24.5 at%. The increasing ratio of O to F atoms confirms that alkalized treatment can effectively reduce F and improve O, which is beneficial to the enhancement of  $\text{NH}_3$  gas sensing. This result is consistent with a previous report [31]. Also, the increase in O 1s also confirms that the numbers of -O or -OH functional groups are increasing on the surface of the alkalized  $\text{Ti}_3\text{C}_2\text{T}_x$ . As shown in Figure 6b,f of the O 1s spectra, there are two peaks at 530.4 eV and 532.2 eV assigned to Ti-O and C-Ti-Ox bonds, respectively. Remarkably, a Ti-OH peak appears at 532.8 eV for the alkalized  $\text{Ti}_3\text{C}_2\text{T}_x$  MXene, which is not present in the pristine  $\text{Ti}_3\text{C}_2\text{T}_x$  MXene, showing the successful alkalization of the MXene. [30,53,54]. The high-resolution XPS spectra of C 1s and Ti 2p of  $\text{Ti}_3\text{C}_2\text{T}_x$  and  $\text{Ti}_3\text{C}_2\text{T}_x$  alkalinized with 5 M NaOH for 12 h are displayed in Figure 6c,d,g,h, respectively. The peaks observed at 282.5 eV, 284.5 eV, 285.3 eV, and 288.2 eV are attributed to C-Ti, C-C, C-O, and C-F, respectively [37,55–57]. After alkalization, the C-Ti peak vanishes, and the proportion of the peak area attributed to C-O increases from 12% to 18%. This is attributed to the breaking of C atoms between Ti atoms and the bonding of C with O on the surface of the alkalized  $\text{Ti}_3\text{C}_2\text{T}_x$  [58], which indicates an increase in -OH groups in the alkalized  $\text{Ti}_3\text{C}_2\text{T}_x$  [59]. The binding energy in the Ti 2p XPS spectra is located at 455.1, 456.8, and 460.7 eV, corresponding to Ti 2p<sub>3/2</sub>, while those at 460.7, 462.1, and 464.5 eV correspond to Ti 2p<sub>1/2</sub>, which represent contributions from C-Ti<sup>2+</sup>(O/OH), C-Ti-F<sub>x</sub>, and TiO<sub>2</sub> [31,54,60]. The percentage of the peak area corresponding to Ti 2p<sub>3/2</sub> at 456.8 eV and Ti 2p<sub>1/2</sub> at 462.1 eV from C-Ti-F<sub>x</sub> of the alkalized  $\text{Ti}_3\text{C}_2\text{T}_x$  MXene significantly decreased from 9.1% to 6.6% and from 8.1% to 1.98%, respectively, in comparison to that of  $\text{Ti}_3\text{C}_2\text{T}_x$  MXene. This is attributed to the decrease in -F functional terminal groups after alkalization. On the other hand, it can be observed that the peaks of Ti 2p<sub>3/2</sub> at 455.1 eV and Ti 2p<sub>1/2</sub> at 460.7 eV from C-Ti<sup>2+</sup>(O/OH) decreased, while Ti 2p<sub>3/2</sub> at 458.8 eV and Ti 2p<sub>1/2</sub> at 464.5 eV from TiO<sub>2</sub> increased after alkalization, indicating that Ti ions are further oxidized during the alkalization process. Overall, all the results showed an increase in the oxygen-to-fluorine atom ratio on the surface after the alkalization of  $\text{Ti}_3\text{C}_2\text{T}_x$ .

Figure 7 shows the elemental EDS mappings of C, O, F, Ti, and Na and the corresponding SEM images of  $\text{Ti}_3\text{C}_2\text{T}_x$  and  $\text{Ti}_3\text{C}_2\text{T}_x$  alkalinized with 5 M NaOH for 12 h. The uniform distributions of C, O, F, Ti, and Na on the surface of both pristine and alkalized  $\text{Ti}_3\text{C}_2\text{T}_x$  are evident. No Al signal is observed, indicating that the Al layers were removed in the process. The results also show the intercalation of Na<sup>+</sup>, the reduction in F elements, and the increase in O elements in the alkalized  $\text{Ti}_3\text{C}_2\text{T}_x$ , which is in agreement with the XPS result. Figure 8 displays a statistical graph of the Na, O, F, Ti, and C element ratio and the O/F ratio of the alkalized  $\text{Ti}_3\text{C}_2\text{T}_x$  (5 M NaOH for 6, 12, 18, 24 h, 2/5/8 M NaOH for 12 h). The  $\text{Ti}_3\text{C}_2\text{T}_x$  alkalinized with 5 M NaOH for 12 h shows the highest O/F ratio. It should be noted that the -OH surface functional terminal groups will become saturated if the concentration of NaOH is too high and the alkalization time is too long. This will induce negative effects on gas sensitivity. Therefore, the dynamic sensing results indicate that an optimal NaOH concentration and alkalization time can be achieved, with the best response characteristics shown by the sensors based on  $\text{Ti}_3\text{C}_2\text{T}_x$  MXene alkalinized with 5 M NaOH.

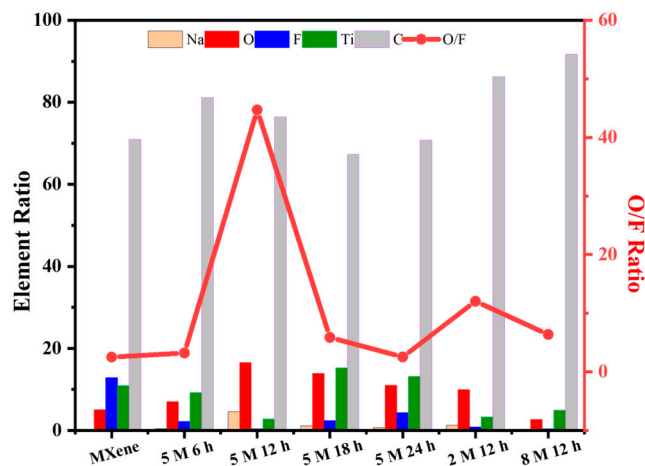


**Figure 8.** The statistical graph of Na, O, F, Ti, and C element ratio and O/F ratio of  $\text{Ti}_3\text{C}_2\text{T}_x$ , alkalinized  $\text{Ti}_3\text{C}_2\text{T}_x$  (5 M NaOH for 6, 12, 18, 24 h, 2/5/8 M NaOH for 12 h).

#### 4. Conclusions

In summary, alkalinized  $\text{Ti}_3\text{C}_2\text{T}_x$  MXene were successfully prepared with different concentrations of NaOH solutions (2, 5, and 8 M) for varying duration (6, 12, 18, and 24 h). Compared to untreated  $\text{Ti}_3\text{C}_2\text{T}_x$  MXene, sensors based on the alkalinized  $\text{Ti}_3\text{C}_2\text{T}_x$  MXene exhibited significantly improved gas-sensing performance, as well as enhanced repeatability and stability upon exposure to  $\text{NH}_3$  at RT and an RH of 40%. This improvement in ammonia-sensing capability can be attributed to the incorporation of  $\text{Na}^+$  metal ions into the MXene layer, leading to an increase in the specific surface area of each layer and in the contact area with  $\text{NH}_3$ . Consequently, such structural modification further enhanced the adsorption and desorption capacity for ammonia. Additionally, the introduction of -OH groups during alkalization led to an increase in the oxygen/fluorine atom ratio. Furthermore, an optimal NaOH concentration and alkalization duration were identified, with  $\text{Ti}_3\text{C}_2\text{T}_x$  MXene sensors alkalinized by 5 M NaOH exhibiting the highest response in this study. Our findings underscore the effectiveness of the alkalization method in enhancing the performance of  $\text{NH}_3$  detection at RT and an RH of 40%, thus facilitating the practical application of  $\text{Ti}_3\text{C}_2\text{T}_x$  MXene in gas sensors.

**Author Contributions:** Methodology, Y.T. and J.X.; Validation, W.Z. and C.L.; Investigation, L.L. and X.S.; Data curation, Y.T. and J.X.; Writing—original draft, Y.T.; Writing—review and editing, J.X. and Q.L.; Visualization, Y.C.; Supervision, J.X. All authors have read and agreed to the published version of the manuscript.

**Funding:** This work was supported by the National Natural Science Foundation of China (No. 62204080), the National Key Research and Development Program Project “China-Sudan Joint Laboratory on a Novel Photovoltaic Ecological Agriculture” (No. 2023YFE0126400), the Hubei Province Introduction of Foreign Talent and Intelligence Project “key Technology Research on Intelligent and Efficient Photovoltaic Ecological Agriculture System” (No. 2023DJC027), the Ministry of Science and Technology, the China–Africa Partner Research Institute Exchange Project “China-South Africa Advanced Photovoltaic Hydrogen Energy System Research Center”, and the National “111 Research Center” for Microelectronics and Integrated Circuits.

**Data Availability Statement:** All data are contained within the article.

**Conflicts of Interest:** The authors declare no conflicts of interest.

#### References

- Grabowski, K.; Srivatsa, S.; Vashisth, A.; Mishnaevsky, L.; Uhl, T. Recent advances in MXene-based sensors for Structural Health Monitoring applications: A review. *Measurement* **2022**, *189*, 110575. [[CrossRef](#)]
- Qin, R.; Shan, G.; Hu, M.; Huang, W. Two-dimensional transition metal carbides and/or nitrides (MXenes) and their applications in sensors. *Mater. Today Phys.* **2021**, *21*, 100527. [[CrossRef](#)]

3. Tai, H.; Wang, S.; Duan, Z.; Jiang, Y. Evolution of breath analysis based on humidity and gas sensors: Potential and challenges. *Sens. Actuators B Chem.* **2020**, *318*, 128104. [[CrossRef](#)]
4. Zhu, S.; Wang, D.; Li, M.; Zhou, C.; Yu, D.; Lin, Y. Recent advances in flexible and wearable chemo- and bio-sensors based on two-dimensional transition metal carbides and nitrides (MXenes). *Mater. Chem. B* **2022**, *10*, 2113–2125. [[CrossRef](#)] [[PubMed](#)]
5. Mirzaei, A.; Le, M.H.; Safaeian, H.; Kim, T.-U.; Kim, J.-Y.; Kim, H.W.; Kim, S.S. Room Temperature Chemiresistive Gas Sensors Based on 2D MXenes. *Sensors* **2023**, *23*, 8829. [[CrossRef](#)] [[PubMed](#)]
6. Moseley, P.T. Progress in the development of semiconducting metal oxide gas sensors: A review. *Meas. Sci. Technol.* **2017**, *28*, 082001. [[CrossRef](#)]
7. Dey, A. Semiconductor metal oxide gas sensors: A review. *Mater. Sci. Eng. B* **2018**, *229*, 206–217. [[CrossRef](#)]
8. Zhang, J.; Li, G.; Liu, J.; Liu, Y.; Yang, R.; Li, L.; Zhao, Q.; Gao, J.; Zhu, G.; Zhu, B.; et al. Metal–organic framework-derived mesoporous rGO–ZnO composite nanofibers for enhanced isopropanol sensing properties. *Sens. Actuators B Chem.* **2023**, *378*, 133108. [[CrossRef](#)]
9. Lee, E.; VahidMohammadi, A.; Prorok, B.C.; Yoon, Y.S.; Beidaghi, M.; Kim, D.-J. Room temperature Gas sensing of two-dimensional titanium carbide (MXene). *J. ACS Appl. Mater. Interfaces* **2017**, *9*, 37184–37190. [[CrossRef](#)]
10. Chen, H.; Chen, Y.; Zhang, H.; Zhang, D.; Zhou, P.; Huang, J. Suspended SnS<sub>2</sub> Layers by Light Assistance for Ultrasensitive Ammonia Detection at Room Temperature. *Adv. Funct. Mater.* **2018**, *28*, 1801035. [[CrossRef](#)]
11. Yu, Z.; Wang, B.; Li, Y.; Kang, D.; Chen, Z.; Wu, Y. The effect of rigid phenoxyl substituent on the NH<sub>3</sub>-sensing properties of tetra- $\alpha$ -(4-tert-butylphenoxy)-metallophthalocyanine/reduced graphene oxide hybrids. *RSC Adv.* **2017**, *7*, 22599–22609. [[CrossRef](#)]
12. Naguib, M.; Mochali, V.N.; Barsoum, M.W.; Gogotsi, Y. 25th anniversary article: MXenes: A new family of two-dimensional materials. *Adv. Mater.* **2014**, *26*, 992–1005. [[CrossRef](#)] [[PubMed](#)]
13. Goel, N.; Kushwah, A.; Kumar, M. Two-dimensional MXenes: Recent emerging applications. *J. RSC Adv.* **2022**, *12*, 25172–25193. [[CrossRef](#)] [[PubMed](#)]
14. Li, J.; Chen, X.; Zhu, X.; Jiang, Y.; Chang, X.; Sun, S. Two-dimensional transition metal MXene-based gas sensors: A review. *Chin. Chem. Lett.* **2024**, *35*, 108286. [[CrossRef](#)]
15. Bhardwaj, R.; Hazra, A. MXene-based gas sensors. *J. Mater. Chem. C* **2021**, *9*, 15735–15754. [[CrossRef](#)]
16. Li, Q.; Li, Y.; Zeng, W. Preparation and Application of 2D MXene-Based Gas Sensors: A Review. *Chemosensors* **2021**, *9*, 225. [[CrossRef](#)]
17. Reddy, M.S.B.; Aich, S. Recent progress in surface and heterointerface engineering of 2D MXenes for gas sensing applications. *Coord. Chem. Rev.* **2024**, *500*, 215542. [[CrossRef](#)]
18. Liu, Z.; Han, D.; Liu, L.; Li, D.; Han, X.; Chen, Y.; Liu, X.; Zhuo, K.; Cheng, Y.; Sang, S. Ultrasensitive ammonia gas sensor based on Ti<sub>3</sub>C<sub>2</sub>T<sub>x</sub>/Ti<sub>3</sub>AlC<sub>2</sub> planar composite at room temperature. *Sens. Actuators B Chem.* **2023**, *378*, 133149. [[CrossRef](#)]
19. Ljubek, G.; Kralj, M.; Roković, M.K. Fluorine-free mechanochemical synthesis of MXene. *Mater. Sci. Technol.* **2023**, *39*, 1645–1649. [[CrossRef](#)]
20. Báez, L.R.D.J.; Rosas, A.S.; Mahale, P.; Mallouk, T.E. Chelation-Based Route to Aluminum-Free Layered Transition Metal Carbides (MXenes). *ACS Omega* **2023**, *8*, 41969–41976. [[CrossRef](#)]
21. Tang, Y.; Yang, C.; Que, W. A novel two-dimensional accordion-like titanium carbide (MXene) for adsorption of Cr(VI) from aqueous solution. *J. Adv. Dielectr.* **2018**, *8*, 1850035. [[CrossRef](#)]
22. Liang, R.; Zhong, L.; Zhang, Y.; Tang, Y.; Lai, M.; Han, T.; Wang, W.; Bao, Y.; Ma, Y.; Gan, S.; et al. Directly Using Ti<sub>3</sub>C<sub>2</sub>T<sub>x</sub> MXene for a Solid-Contact Potentiometric pH Sensor toward Wearable Sweat pH Monitoring. *Membranes* **2023**, *13*, 376. [[CrossRef](#)] [[PubMed](#)]
23. Alhabeib, M.; Maleski, K.; Anasor, B.; Lelyukh, P.; Clark, L.; Sin, S.; Gogotsi, Y. Guidelines for Synthesis and Processing of Two-Dimensional Titanium Carbide (Ti<sub>3</sub>C<sub>2</sub>T<sub>x</sub> MXene). *Chem. Mater.* **2017**, *29*, 7633–7644. [[CrossRef](#)]
24. Wang, Y.; Fu, J.; Xu, J.; Hu, H.; Ho, D. Atomic Plasma Grafting: Precise Control of Functional Groups on Ti<sub>3</sub>C<sub>2</sub>T<sub>x</sub> MXene for Room Temperature Gas Sensors. *ACS Appl. Mater. Interfaces* **2023**, *15*, 12232–12239. [[CrossRef](#)] [[PubMed](#)]
25. Fagerli, F.H.; Vullum, P.E.; Grande, T.; Wang, Z.; Selbach, S.M.; Wiik, K.; Wagner, N.P. Bulk substitution of F-terminations from Ti<sub>3</sub>C<sub>2</sub>T<sub>x</sub> MXene by cation pillaring and gas hydrolyzation. *FlatChem* **2023**, *38*, 100470. [[CrossRef](#)]
26. Chen, L.; Bi, Y.; Jing, Y.; Dai, J.; Li, Z.; Sun, C.; Men, A.; Xie, H.; Hu, M. Phosphorus Doping Strategy-Induced Synergistic Modification of Interlayer Structure and Chemical State in Ti<sub>3</sub>C<sub>2</sub>T<sub>x</sub> toward Enhancing Capacitance. *Molecules* **2023**, *28*, 4892. [[CrossRef](#)] [[PubMed](#)]
27. Persson, I.; Näslund, L.-Å.; Halim, J.; Barsoum, M.W.; Darakchieva, V.; Palisaitis, J.; Rosen, J.; Persson, P.O.Å. On the organization and thermal behavior of functional groups on Ti<sub>3</sub>C<sub>2</sub>MXene surfaces in vacuum. *2D Mater.* **2017**, *5*, 015002. [[CrossRef](#)]
28. Zhang, G.; Wang, T.; Xu, Z.; Liu, M.; Shen, C.; Meng, Q. Synthesis of amino-functionalized Ti<sub>3</sub>C<sub>2</sub>T<sub>x</sub> MXene by alkalization-grafting modification for efficient lead adsorption. *Chem. Commun.* **2020**, *56*, 11283–11286. [[CrossRef](#)] [[PubMed](#)]
29. Liang, J.; Zhou, Z.; Zhang, Q.; Hu, X.; Peng, W.; Li, Y.; Zhang, F.; Fan, X. Chemically-confined mesoporous  $\gamma$ -Fe<sub>2</sub>O<sub>3</sub> nanospheres with Ti<sub>3</sub>C<sub>2</sub>T<sub>x</sub> MXene via alkali treatment for enhanced lithium storage. *J. Power Sources* **2021**, *495*, 229758. [[CrossRef](#)]
30. Bae, Y.H.; Park, S.; Noh, J.-S. Control of electrical properties of Ti<sub>3</sub>C<sub>2</sub>T<sub>x</sub> mediated by facile alkalization. *Surf. Interfaces* **2023**, *41*, 103258. [[CrossRef](#)]

31. Yang, Z.; Li, A.; Wang, C.; Liu, F.; He, J.; Li, S.; Wang, J.; You, R.; Yan, X.; Su, P.; et al. Improvement of gas and humidity sensing properties of organ-like MXene by alkaline treatment. *ACS Sens.* **2019**, *4*, 1261–1269. [[CrossRef](#)] [[PubMed](#)]
32. Jin, X.; Yue, S.; Zhang, J.; Qian, L.; Guo, X. Three-Dimensional Vanadium and Nitrogen Dual-Doped  $\text{Ti}_3\text{C}_2$  Film with Ultra-High Specific Capacitance and High Volumetric Energy Density for Zinc-Ion Hybrid Capacitors. *Nanomaterials* **2024**, *14*, 490. [[CrossRef](#)] [[PubMed](#)]
33. Allothman, A.A.; Khan, M.R.; Albaqami, M.D.; Mohandoss, S.; Allothman, Z.A.; Ahmad, N.; Alqahtani, K.N.  $\text{Ti}_3\text{C}_2$ -MXene/NiO Nanocomposites-Decorated  $\text{CsPbI}_3$  Perovskite Active Materials under UV-Light Irradiation for the Enhancement of Crystal-Violet Dye Photodegradation. *Nanomaterials* **2023**, *13*, 3026. [[CrossRef](#)] [[PubMed](#)]
34. Xiang, Y.; Fang, L.; Wu, F.; Zhang, S.; Ruan, H.; Luo, H.; Zhang, H.; Li, W.; Long, X.; Hu, B.; et al. 3D crinkled alk- $\text{Ti}_3\text{C}_2$  MXene based flexible piezoresistive sensors with ultra-high sensitivity and ultra-wide pressure range. *J. Adv. Mater. Technol.* **2021**, *6*, 2001157. [[CrossRef](#)]
35. Sui, J.; Chen, X.; Li, Y.; Peng, W.; Zhang, F.; Fan, X. MXene derivatives: Synthesis and applications in energy convention and storage. *RSC Adv.* **2021**, *11*, 16065–16082. [[CrossRef](#)] [[PubMed](#)]
36. Natu, V.; Pai, R.; Wilson, O.; Gadasu, E.; Badr, H.; Karmakar, A.; Magenau, A.J.D.; Kalra, V.; Barsoum, M.W. Effect of base/nucleophile treatment on interlayer ion intercalation, surface terminations, and osmotic swelling of  $\text{Ti}_3\text{C}_2\text{T}_z$  MXene multilayers. *Chem. Mater.* **2022**, *34*, 678–693. [[CrossRef](#)]
37. Kim, S.J.; Koh, H.-J.; Ren, C.E.; Kwon, O.; Maleski, K.; Cho, S.-Y.; Anasori, B.; Kim, C.-K.; Choi, Y.-K.; Kim, J.; et al. Metallic  $\text{Ti}_3\text{C}_2\text{T}_x$  MXene gas sensors with ultrahigh signal-to-noise ratio. *ACS Nano* **2018**, *12*, 986–993. [[CrossRef](#)]
38. Lee, J.Y.; Kang, Y.C.; Koo, C.M.; Kim, S.J.  $\text{Ti}_3\text{C}_2\text{T}_x$  MXene Nanolaminates with Ionic Additives for Enhanced Gas-Sensing Performance. *ACS Appl. Nano Mater.* **2022**, *5*, 11997–12005. [[CrossRef](#)]
39. Lee, S.H.; Eom, W.; Shin, H.; Ambade, R.B.; Bang, J.H.; Kim, H.W.; Han, T.H. Room-Temperature, Highly Durable  $\text{Ti}_3\text{C}_2\text{T}_x$  MXene/Graphene Hybrid Fibers for  $\text{NH}_3$  Gas Sensing. *ACS Appl. Mater. Interfaces* **2020**, *12*, 10434–10442. [[CrossRef](#)]
40. Yuan, W.; Yang, K.; Peng, H.; Li, F.; Yin, F. A flexible VOCs sensor based on a 3D MXene framework with a high sensing performance. *J. Mater. Chem. A* **2018**, *6*, 18116–18124. [[CrossRef](#)]
41. Yu, H.; Dai, L.; Liu, Y.; Zhou, Y.; Fan, P.; Luo, J.; Zhong, A.  $\text{Ti}_3\text{C}_2\text{T}_x$  MXene-SnO<sub>2</sub> nanocomposite for superior room temperature ammonia gas sensor. *J. Alloys Compd.* **2023**, *962*, 171170. [[CrossRef](#)]
42. Li, X.; Xu, J.; Jiang, Y.; He, Z.; Liu, B.; Xie, H.; Li, H.; Li, Z.; Wang, Y.; Tai, H. Toward Agricultural Ammonia Volatilization Monitoring: A Flexible Polyaniline/ $\text{Ti}_3\text{C}_2\text{T}$  Hybrid Sensitive Films Based Gas Sensor. *Sens. Actuators B Chem.* **2020**, *316*, 128144. [[CrossRef](#)]
43. Wu, M.; He, M.; Hu, Q.; Wu, Q.; Sun, G.; Xie, L.; Zhang, Z.; Zhu, Z.; Zhou, A.  $\text{Ti}_3\text{C}_2$  MXene-Based Sensors with High Selectivity for  $\text{NH}_3$  Detection at Room Temperature. *ACS Sens.* **2019**, *4*, 2763–2770. [[CrossRef](#)] [[PubMed](#)]
44. Yan, H.; Chu, L.; Li, Z.; Sun, C.; Shi, Y.; Ma, J. 2H-MoS<sub>2</sub>/ $\text{Ti}_3\text{C}_2\text{T}_x$  MXene composites for enhanced NO<sub>2</sub> gas sensing properties at room temperature. *Sens. Actuators Rep.* **2022**, *4*, 100103. [[CrossRef](#)]
45. Ma, J.; Zhai, H.; Zhang, Z.; Di, M.; Sun, Z.; Zhang, K.; Hu, J.; Fan, H. Three-dimensional alkalized  $\text{V}_2\text{CT}_x$  MXene/ $\text{NH}_2$ -Graphene heterojunction nanocomposites for ammonia detection at room temperature. *ACS Appl. Nano Mater.* **2023**, *6*, 19797–19806.
46. Liu, M.; Ding, Y.; Lu, Z.; Song, P.; Wang, Q. Layered  $\text{Ti}_3\text{C}_2\text{T}_x$  MXene/CuO spindles composites for  $\text{NH}_3$  detection at room temperature. *J. Alloys Compd.* **2023**, *938*, 168563. [[CrossRef](#)]
47. Pasupuleti, K.S.; Thomas, A.M.; Thomas, A.M.; Vidyasagar, D.; Rao, V.N.; Yoon, S.-G.; Kim, Y.-H.; Kim, S.-G.; Kim, M.-D. ZnO/ $\text{Ti}_3\text{C}_2\text{T}_x$  MXene Hybrid Composite-Based Schottky-Barrier-Coated SAW Sensor for Effective Detection of Sub-ppb-Level  $\text{NH}_3$  at Room Temperature under UV Illumination. *ACS Mater. Lett.* **2023**, *5*, 2739–2746. [[CrossRef](#)]
48. Zheng, W.; Zhang, P.; Tian, W.; Qin, X.; Zhang, Y.; Sun, Z. Alkali treated  $\text{Ti}_3\text{C}_2\text{T}_x$  MXenes and their dye adsorption performance. *Mater. Chem. Phys.* **2018**, *206*, 270–276.
49. Wang, R.; Cao, H.; Yao, C.; Peng, C.; Qiu, J.; Dou, K.; Tsidaeva, N.; Wang, W. Construction of alkalized MXene-supported  $\text{CoFe}_2\text{O}_4$ /CS composites with super-strong adsorption capacity to remove toxic dyes from aqueous solution. *J. Appl. Surf. Sci.* **2023**, *624*, 157091. [[CrossRef](#)]
50. Lian, P.; Dong, Y.; Wu, Z.; Zheng, S.; Wang, X.; Wang, S.; Sun, C.; Qin, J.; Shi, X.; Bao, X. Alkalized  $\text{Ti}_3\text{C}_2$  MXene nanoribbons with expanded interlayer spacing for high-capacity sodium and potassium ion batteries. *Nano Energy* **2017**, *40*, 1–8. [[CrossRef](#)]
51. Chen, J.; Qin, W.; Li, K.; Feng, L.; Chen, J.; Qiao, H.; Yang, M.; Tian, Z.; Li, X.; Gu, C.; et al. A high-sensitivity, fast-response and high-stability humidity sensor of curly flake  $\text{Ti}_3\text{C}_2\text{T}_x$  MXene prepared by electrolytic intercalation of NaOH solution. *J. Mater. Chem. A* **2022**, *10*, 22278–22288. [[CrossRef](#)]
52. Xiao, B.; Li, Y.; Yu, X.; Cheng, J. MXenes: Reusable materials for  $\text{NH}_3$  sensor or capturer by controlling the charge injection. *Sens. Actuators B Chem.* **2016**, *235*, 103–109. [[CrossRef](#)]
53. Näslund, L.-Å.; Persson, I. XPS spectra curve fittings of  $\text{Ti}_3\text{C}_2\text{T}_x$  based on first principles thinking. *Appl. Surf. Sci.* **2022**, *593*, 153442. [[CrossRef](#)]
54. Natu, V.; Benchakar, M.; Canaff, C.; Habrioux, A.; Célérier, S.; Barsoum, M.W. A critical analysis of the X-ray photoelectron spectra of  $\text{Ti}_3\text{C}_2\text{T}_z$  MXenes. *Matter* **2021**, *4*, 1224–1251. [[CrossRef](#)]
55. Halim, J.; Cook, K.M.; Naguib, M.; Eklund, P.; Gogotsi, Y.; Rosen, J.; Barsoum, M.W. X-ray photoelectron spectroscopy of select multi-layered transition metal carbides (MXenes). *Appl. Surf. Sci.* **2016**, *362*, 406–417. [[CrossRef](#)]

56. Ghidiu, M.; Halim, J.; Kota, S.; Bish, D.; Gogotsi, Y.; Barsoum, M.W. Ion-exchange and cation solvation reactions in  $Ti_3C_2$  MXene. *Chem. Mater.* **2016**, *28*, 3507–3514. [[CrossRef](#)]
57. Ma, S.; Guo, J.; Zhang, H.; Shao, X.; Zhang, D. A Room Temperature Trimethylamine Gas Sensor Based on Electrospun Molybdenum Oxide Nanofibers/ $Ti_3C_2T_x$  MXene Heterojunction. *Nanomaterials* **2024**, *14*, 537. [[CrossRef](#)] [[PubMed](#)]
58. Chen, W.; Tan, J.; Cheng, P.; Ai, Y.; Xu, Y.; Ye, N. 3D porous MXene ( $Ti_3C_2T_x$ ) prepared by alkaline-induced flocculation for supercapacitor electrodes. *Materials* **2022**, *15*, 925. [[CrossRef](#)] [[PubMed](#)]
59. Ma, W.; Tang, H.; Li, T.; Wang, L.; Zhang, L.; Yu, Y.; Qiao, Z.; Liu, W. Research about the capacitance properties of ion-induced multilayer and self-assembled monolayer  $Ti_3C_2T_x$ . *RSC Adv.* **2022**, *12*, 3554–3560. [[CrossRef](#)]
60. Limbu, T.B.; Chitar, B.; Orlando, J.D.; Cervantes, M.Y.G.; Kumari, S.; Li, Q.; Tang, Y.G.; Yan, F. Green synthesis of reduced  $Ti_3C_2T_x$  MXene nanosheets with enhanced conductivity, oxidation stability, and SERS activity. *J. Mater. Chem. C* **2020**, *8*, 4722–4731. [[CrossRef](#)]

**Disclaimer/Publisher’s Note:** The statements, opinions and data contained in all publications are solely those of the individual author(s) and contributor(s) and not of MDPI and/or the editor(s). MDPI and/or the editor(s) disclaim responsibility for any injury to people or property resulting from any ideas, methods, instructions or products referred to in the content.